文章编号：1001-9014(2020)02-0228-07

DOI:10.11972/j.issn.1001-9014.2020.02.010

Human localization technology based on the pyroelectric infrared sensors

WU Qin-Qin[1], LI Xi-Cai[1], WANG Yuan-Qing[1,2*], REN Shu-Ping[3]

(1. School of Electronic Science and Engineering, Nanjing University, Nanjing 210023, China;
2. Key Laboratory of Intelligent Optical Sensing and Manipulation, Ministry of Education, Nanjing University, Nanjing 210023, China;
3. JiangXi Academy of Sciences, Nanchang 330000, China.)

Abstract: A field of views of pyroelectric infrared sensors modulation strategy is proposed. The strategy can improve the human localization resolution, and it will not reduce the detection distance of pyroelectric infrared sensor. For the strategy, the field of views of pyroelectric infrared sensors are modulated by a mask. And the modulated field of views overlap and interleave with each other to form some sampling areas. In order to verify the proposed field of views modulation strategy, the human localization node which includes nine pyroelectric infrared sensors is fabricated. The modulated degree of the field of views of each pyroelectric infrared sensor is 36°. The degree of each sampling area is 4°. If the human moves in a sampling area, the corresponding pyroelectric infrared sensors will be triggered. The human position can be localized by using at least two nodes. According to the states of the pyroelectric infrared sensors, the human position can be estimated. In the experiment, two nodes are set in a 600 cm × 600 cm square area, the theoretical error is analyzed by using least square estimation. The theoretical maximum error of the two nodes human localization equipment in a 600 cm×600 cm square area is about 70 cm. Eight human positions are estimated in experiments, and the estimation route is formed by connecting all the estimated positions. The estimation route is close to the predefined route. The minimum and maximum estimation errors are about 4. 42 cm and 16. 91 cm respectively.

Key words: pyroelectric infrared sensor, human position localization, least square estimation
PACS: 07. 60. -j, 42. 79. -e

基于热释电红外探测器的人体定位技术

吴勤勤[1], 李希才[1], 王元庆[1,2*], 任舒平[3]

(1. 南京大学 电子科学与工程学院,江苏 南京 210023;
2. 南京大学 智能光感知与调控技术教育部重点实验室,江苏 南京 210023;
3. 江西省科学院,江西 南昌 330000)

摘要:提出了一种热释电红外探测器视场调制策略。此策略能够提高人体定位分辨率,并且不会降低探测器的探测距离。对于此策略,热释电红外探测器的视场被遮光板调制,且调制后的探测器视场相互重叠交错形成一些采样区域。为了验证此策略,制作了包含九个热释电红外探测器的人体定位节点,节点中所有调制后的探测器视场角均为36°,每一个采样区域的角度均为4°。如果受测者在一个采样区域中运动,对应的热释电红外探测器将被触发,至少需要两个人体定位节点才能实现人体定位。根据节点中热释电红外探测器的状态,能够估计人体的位置。实验中,在600 cm × 600 cm的方形区域内设置两个人体定位节点,使用最小二乘法估计理论误差,其最大理论误差为70 cm。实验中估计了八个人体位置,将所有的估计位置点连接起来形成估计路径。估计路径与预设路径十分接近。实验中的最小和最大定位误差分别为4.42 cm和16.91 cm。

关 键 词:热释电红外探测器;人体定位;最小二乘法

Received date: 2019-05-24, **revised date**: 2019-11-24 **收稿日期**:2019-05-24,**修回日期**:2019-11-24

基金项目:国家重点研发计划(2016YFB0401500), 江苏省重点研发计划 (BE2016173),南京大学优秀博士研究生创新能力提升计划B

Foundation items: Supported by the National Key R&D Plan (2016YFB0401500), R&D Plan of Jiangsu Science and Technology Department (BE2016173), and Program B for Outstanding PhD Candidate of Nanjing University

作者简介(biography): 吴勤勤(1991-), 男, 江西南昌人,博士研究生. 主要研究领域为热释电红外探测器及其应用、激光雷达系统及相关算法. E-mail: wuqinqingreat@sina.com

*通信作者(*Corresponding author): E-mail: yqwang@nju.edu.cn

中图分类号:TN219　　文献标识码:A

Introduction

Human tracking and localization technology is one of most significant topic for the security [1] and machine vision [2]. Researchers have done a lot of work for the human localization and tracking. There are some kinds of strategy for human tracking and localization. The first strategy utilizes vision device to detect the target, such as visible-light camera and near-infrared camera [3]. The visible-light camera and near-infrared camera can quick and precise to find targets based on the computer vision and digital image processing techniques [4]. But the environment factors such as high light background or weak light condition will affect the detection. And not all occasions are suitable for installation of camera, such as bedroom or toilet. In addition, the near-infrared camera need to use the near infrared source for illumination. The detection range of near-infrared camera is limited by the limitation of source illumination range. The second strategy is based on wearable device. This method requires target human to wear a device on his glasses or collar, such as near-infrared led. And this method uses a detector such as position sensitive device (PSD) to track the wearable device [5]. However, the power unit for the wearable device cannot work for a long time, and the wearable device will lead to discomfort. The dense sensing based activity monitoring is the third strategy, such as environment state-change sensors [6], break-beam sensors, pressure mats, contact switches [7], microphones and pyroelectric infrared sensors. The dense sensing is suitable for intelligent environment enabled applications [8].

Pyroelectric infrared sensors (PIR) [9-11] received extensive attention due to the low cost, low power consumption and excellent performances. The PIR can detect the mid-infrared light (8~14 μm) emitted by human body. Thus, the PIR can detect the human body without any help of other light source, and the human body doesn't need to equip any device. Furthermore, the detection based on the PIR doesn't belong to the imaging detection. Thus, it won't invade human privacy. It is suitable for most occasions. And the PIR only can be triggered by the dynamic changed light. The invariable light or heater in the field of views (FOVs) cannot trigger the sensor. Thus, the localization system composed by PIRs can avoid disturbances caused by the obstacles.

In this paper, a FOV modulation strategy is proposed, and the human localization node based on the proposed strategy is fabricated. The proposed FOVs modulation strategy can improve the human localization resolution without reduction of the detection distance of the PIR. Owing to larger angle of modulated FOV and smaller angle of sampling area (SA), the modulation strategy can achieve larger theoretical detection distance and higher angle resolution compare with the strategies which are reported in [12-14]. For our node, the angle of the modulated FOV of each PIR is 36°, and the angle of each SA is 4°. We use two nodes to localize the human position in a 600 cm×600 cm square area, and the theoretical error is analyzed. The maximum theoretical error is about 70 cm. For the experiment, the minimum and maximum localization errors are about 4.42 cm and 16.91cm respectively.

1　The principle of human localization by use of PIR

PIR is a frequently-used human body detection device. It is sensitive to 8~14 μm infrared light. The Fresnel lens can enhance the detection distance of PIR. If a human walks in the FOV of the PIR, the PIR will be triggered and output analog signal. Process the signal to determine the state of the PIR. Use the '0' and '1' (two states) to represent the PIRs are triggered or not [13,15]. According the states of the PIRs, the position of the human can be estimated. Some papers have been reported that use the PIRs to localize human position. In Ref. 12, fourteen separate masks are used to modulate the FOVs of fourteen PIRs, the angle of the SA for each PIR is set to 5°, the sketch map of the modulation strategy can be seen in Fig. 1(a). In Refs. 13-14, researchers use a mask to modulate the FOV of one PIR. The modulation strategy is shown in Fig. 1(b).

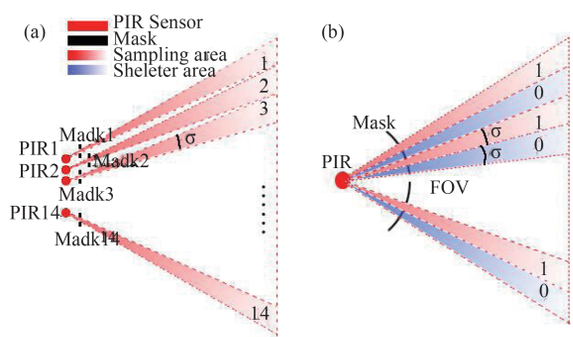

Fig. 1　The sketch map of the modulation strategy of Ref. 12 and Refs. 13-14 (a) The modulation strategy of Ref. 12, (b) the modulation strategy of Refs. 13-14
图1　文献[12]及[13-14]中所使用的调制策略示意图(a)文献[12]所使用的调制策略,(b)文献[13-14]所使用的调制策略

As shown in Fig. 1(a-b), the σ represents the angle resolution. Obviously, for these two kinds of modulation strategies, the smaller degree of FOV of PIR is, the higher angle resolution of system can be achieved. However, the smaller degree of FOV is, the less infrared energy the PIR can receive. It will impact the detection distance of the PIR. The sketch map of the proposed FOVs modulation strategy can be seen in Fig. 2.

As shown in Fig. 2(a), there is a rectangular window on the mask, and it can modulate the FOV of the PIR. The projection of the modulated FOV on *X*-*Y* plane

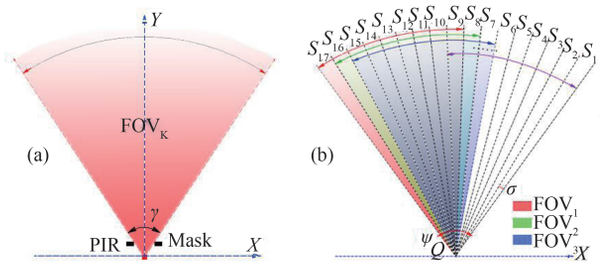

Fig. 2 The sketch map of the proposed FOVs modulation strategy (a) the FOV of one PIR is modulated by a mask, (b) ideally, the starting points of the FOVs of multiple PIRs are located at same point (Q), and the FOVs stagger and overlap with each other to form multiple SAs.

图2 提出的视场调制策略示意图 (a) 遮光板调制单个热释电红外探测器的视场, (b) 理想情况下,多个热释电红外探测器视场的起点位于同一点(Q),并且这些视场相互交错重叠形成多个采样区域。

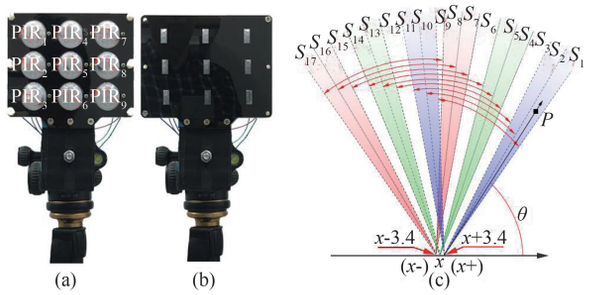

Fig. 3 The physical map of the node, and the sketch map of the sampling areas in non-ideal case (a) The arrangement of PIRs, (b) the physical map of whole node, (c) the sketch map of the sampling areas of the node in non-ideal case

图3 节点实物图及非理想情况下采样区域示意图 (a) 热释电红外探测器的排布示意图,(b) 整个节点的实物图,(c) 非理想情况下采样区域示意图。

is a fan-shaped. Set the angle of the projection to be γ. In order to achieve human position localization, multiple PIRs should be used. In this paper, we describe the proposed modulation strategy based on the node which includes nine PIRs. The FOVs are labeled as FOV_k (k=1, 2, 3, ……, K, K=9). The FOVs of PIRs interleave and overlap with each other to form multiple SAs, as shown in Fig. 2(b). Ideally, assume that all the PIRs are located at same point (Q). Thus, the starting points of all FOVs are also located at this point.

Set the angle of the detection area of the node which includes K PIRs to be ψ, as shown in Fig. 2(b). The SAs are labeled as S_l (l=1, 2, 3, ……, L). The angle σ of each SA can be described in Eq. 1:

$$\sigma = \frac{\psi}{L} \quad , \quad (1)$$

where L is the total number of SAs. And for the proposed strategy, ψ also can be described as Eq. 2:

$$\psi = 2\gamma - \sigma = \frac{2L\gamma}{L+1} \quad . \quad (2)$$

The relationship between K and L can be described as Eq. 3:

$$L = 2K - 1 \quad . \quad (3)$$

Substitute the Eq. 2 and Eq. 3 into Eq. 1, the $\sigma = \gamma/K$ can be obtained. For the proposed modulation strategy, the angle resolution σ is related to γ and K. If the γ is given, we can increase the K to improve the angle resolution, and the γ doesn't need to be reduced. In order to verify the proposed modulation strategy, the human localization node which include nine PIRs is fabricated, as shown in Fig. 3(a) and Fig. 3(b). For the node, the γ is equal to 36°, the ψ is equal to 68°, L is equal to 17, the σ is equal to 4°. In addition, for the node and the proposed modulation strategy, the maximum detection distance of each PIR is about 7 m.

For the node, the PIRs (KP500B, Nisaila. The parameters of the KP500B can be seen in Table. 1) are arranged in 3x3 matrix, the horizontal distance between adjacent PIRs is 3.4cm. The arrangement of PIRs are shown in Fig. 3(a). The angle of the original FOV of the PIR with Fresnel lens is about 100°. The nine windows on the mask and the nine PIRs are corresponding one by one. As shown in Fig. 3, it is impossible to set all detectors at the same point. The PIR_1~PIR_3 move 3.4cm toward to left relative to PIR_4~PIR_6, and the PIR_7~PIR_9 move 3.4cm toward to right relative to the PIR_4~PIR_6. As shown in Fig. 3(c), if the X axis coordinates of starting points of the FOVs of PIR_4~PIR_6 are x, the X axis coordinates of starting points of the FOVs of the PIR_1~PIR_3 and the PIR_7~PIR_9 are x+3.4 and x-3.4 respectively. Of course, the angles of the FOVs and the SAs remain unchanged despite the movement of FOVs.

Table 1 The parameters of the KP500B
表1 KP500B的参数

Item	Parameters
Pass Band	5~14 μm
Transmittance of the filter	>75%
Sensitivity	3 300 V/W
Detectivity	1.5×108 cm·Hz1/2·W−1
Noise	<200 mV (mVp-p, 25℃)

When human walks into different sampling area, the different combination of '0' and '1' sequence can be got. Thus, the '0' and '1' sequence can indicate which SA the human located in. The codes of SAs are list in Table 2.

If the human located in a SA, we can think that the SA is 'triggered'. Assume a human located in S_l, and only the S_l is 'triggered'. We can assume that the human is moving at the angular bisector line A_l of the S_l. Such as the point P which is locate at A_l, as shown in Fig. 3(c). The angle θ between the A_l and X axis can be described in Eq. 4 [15].

$$\theta = \frac{\pi - \psi}{2} + \frac{\psi}{L} l - \frac{\psi}{2L} \quad . \quad (4)$$

It should be noted that there is no case that multiple SAs are triggered simultaneously for the proposed modulation strategy. However, the human body may cover multiple SAs or the human body only covers one SA, and

Table 2　The codes scheme of the 17-SAs.
表2　17个采样区域的编码序列

SA	The state of PIR									Sequence
	1	2	3	4	5	6	7	8	9	
1	1	0	0	0	0	0	0	0	0	100000000
2	1	1	0	0	0	0	0	0	0	110000000
3	1	1	1	0	0	0	0	0	0	111000000
……					……					……
15	0	0	0	0	0	0	1	1	1	000000111
16	0	0	0	0	0	0	0	1	1	000000011
17	0	0	0	0	0	0	0	0	1	000000001

he (she) makes minor motion. In these case, the multiple SAs can take turn to be triggered. Assume these SAs are S_l, S_{l+1}, ……, S_{l+m}, we can think that the human is located at the angular bisector line of the area which consists of S_l, S_{l+1}, ……, S_{l+m}. The θ can be described in Eq. 5:

$$\theta = \frac{\pi - \psi}{2} + \frac{\psi}{L} m - \frac{\psi}{2L} (m - l + 1) \quad . \quad (5)$$

In order to further verify the proposed modulation strategy. We use the node to localize the human position. At least two nodes are required for localization. Assume that there are two nodes are set in a square area (600 cm×600 cm), as shown in Fig. 4. The symmetry axes of the detection areas of the node-1 and node-2 intersect vertically at Q', and they intersect the X and Y axes at $Q_1(300,0)$ and $Q_2(0,300)$ respectively. The valid localization area of two nodes human localization equipment is colored in lilac.

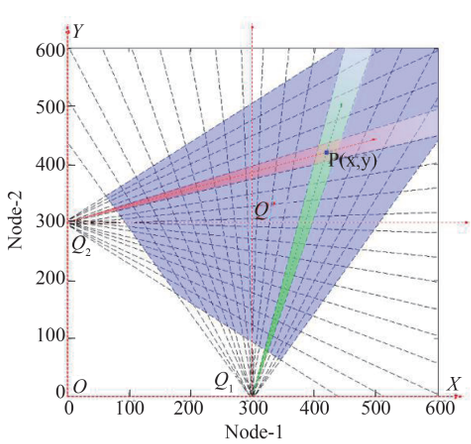

Fig. 4　Two nodes are used for human localization.
图4　两个节点应用于人体定位

Name the 'triggered' SAs S_{il} (i=1, 2). The i is the index of nodes. The angle between angular bisector A_{il} and X axis is named θ_{il}. It should be noticed that, the θ_{1l} and θ_{2l} are equal to θ and $\theta - \pi/2$ respectively, the θ can be calculated by using the Eq. 4 or Eq. 5. According to Fig. 3(c), the coordinates of the intersections (x_{il}, y_{il}) of the A_{il} and X axis or Y axis can be calculated, and they are listed in Table . 3.

The slopes of the angular bisector A_{il} are name k_{il} (if the k_{il} is exist), and they can be described in Eq. 6.

$$k_{il} = \tan\theta_{il} \quad . \quad (6)$$

Table 3　The intersection (x_{il}, y_{il}) of the angular bisector A_{il} and X axis or Y axis.
表3　角平分线A_{il}和X轴或Y轴的交点(x_{il}, y_{il})

The Angular Bisector	x_{il}(cm)	y_{il}(cm)
A_{11}, A_{12}, $A_{1(10)}$, $A_{1(11)}$	300+3.4	0
A_{13}, $A_{1(12)}$	300+1.7	0
A_{14}, A_{15}, $A_{1(9)}$, $A_{1(13)}$, $A_{1(14)}$	300	0
A_{16}, $A_{1(15)}$	300-1.7	0
A_{17}, A_{18}, $A_{1(16)}$, $A_{1(17)}$	300-3.4	0
A_{21}, A_{22}, $A_{2(10)}$, $A_{2(11)}$	0	300-3.4
A_{23}, $A_{2(12)}$	0	300-1.7
A_{24}, A_{25}, A_{29}, $A_{2(13)}$, $A_{2(14)}$	0	300
A_{26}, $A_{2(15)}$	0	300+1.7
A_{27}, A_{28}, $A_{2(16)}$, $A_{2(17)}$	0	300+3.4

And the expressions of the angular bisectors of the 'triggered' SAs can be described in Eq. 7:

$$y_{est} - y_{il} = k_{il}(x_{est} - x_{il}) \quad , \quad (7)$$

where the (x_{est}, y_{est}) is the estimated human position. Substituting the i=1 and i=2 into the Eq. 7. Then the Eq. 8 can be got.

$$\begin{cases} y_{est} - y_{1l} = k_{1l}(x_{est} - x_{1l}) \\ y_{est} - y_{2l} = k_{2l}(x_{est} - x_{2l}) \end{cases} \quad . \quad (8)$$

The Eq. 8 in matrix form can be described in Eq. 9

$$\boldsymbol{Ap} = \boldsymbol{B} \quad , \quad (9)$$

where $\boldsymbol{p} = [x_{est}, y_{est}]^T$, $\boldsymbol{A}$ and $\boldsymbol{B}$ can be described as follows:

$$\boldsymbol{A} = \begin{bmatrix} k_{1l} & -1 \\ k_{2l} & -1 \end{bmatrix}$$

$$\boldsymbol{B} = \begin{bmatrix} k_{1l}x_{1l} - y_{1l} \\ k_{2l}x_{2l} - y_{2l} \end{bmatrix}$$

The human position P can be calculated by Eq. 10:

$$\begin{aligned} x_{est} &= \frac{y_{2l} - y_{1l} + k_{1l}x_{1l} - k_{2l}x_{2l}}{k_{1l} - k_{2l}} \\ y_{est} &= \frac{k_{1l}(k_{2l}x_{1l} - x_{2l}) + k_{1l}y_{2l} - k_{2l}y_{1l}}{k_{1l} - k_{2l}} \end{aligned} \quad . \quad (10)$$

Substituting the values of k_{il} and the corresponding (x_{il}, y_{il}) which are listed in Table 3 into Eq. 10, the human position can be calculated. In addition, the k_{1l} may not exist. In this case, the $x_{est}=x_{1l}=300$. And substitute it into Eq. 8. The $y_{est}=y_{2l}+k_{2l}(300-x_{2l})$ can be obtained.

2 The estimation error analysis

The errors result from the hypothesis that the human is located at the angular bisector of the 'triggered' SA. The estimation human position is (x_{est}, y_{est}). Assuming the errors of x_{est}, y_{est} are Δx, Δy respectively. Thus, the real coordinate of the human position (x, y) can be described in Eq. 11:

$$\begin{cases} x_{est} = x - \Delta x \\ y_{est} = y - \Delta y \end{cases} . \quad (11)$$

Substituting the Eq. 11 into the Eq. 8, the Eq. 12 can be got.

$$\begin{cases} k_{1l}\Delta x - \Delta y = k_{1l}x - k_{1l}x_{1l} - y + y_{1l} \\ k_{2l}\Delta x - \Delta y = k_{2l}x - k_{2l}x_{2l} - y + y_{2l} \end{cases} . \quad (12)$$

Set the $\Delta \boldsymbol{p} = [\Delta x, \Delta y]^{\mathrm{T}}$. The matrix form of Eq. 12 is shown in Eq. 13:

$$\boldsymbol{C}\Delta \boldsymbol{p} = \Delta \boldsymbol{b} , \quad (13)$$

where the $\boldsymbol{C}$ and $\Delta \boldsymbol{b}$ are described as follows:

$$\boldsymbol{C} = \begin{bmatrix} k_{1l} & -1 \\ k_{2l} & -1 \end{bmatrix}$$

$$\Delta \boldsymbol{b} = \begin{bmatrix} k_{1l}x - k_{1l}x_{1l} - y + y_{1l} \\ k_{2l}x - k_{2l}x_{2l} - y + y_{2l} \end{bmatrix}$$

The least square estimation for error can be described in Eq. (14):

$$\Delta \boldsymbol{p} = (\boldsymbol{C}^{\mathrm{T}}\boldsymbol{C})^{-1}\boldsymbol{C}^{T}\Delta \boldsymbol{b} . \quad (14)$$

And if the k_{1l} does not exists, the $x_{1l}=300$. Thus, the $\Delta x=0$, $\Delta y=y-y_{2l}+k_{2l}x_{2l}-k_{2l}x$, and it can be simplified to $\Delta y = y - y_{2l} - k_{2l}x$.

According to the formulas mentioned above, the localization error of two nodes human localization equipment can be calculated by using the numerical simulation. The error is shown in Fig. 5(a) and Fig. 5(b).

It can be seen from Fig. 5(a-b), the farther away from two nodes, the larger localization error is. And as shown in Fig. 5(a), in the quadrilateral which is formed by intersections of two SAs of two nodes, the farther away from the intersection of the two angular bisectors, the larger localization error is. The maximum theoretical error of the two nodes human localization equipment in 600 cm×600 cm square area is about 70 cm, as shown in Fig. 5(b). We only analyze the error in the case that the human only 'trigger' one SA of a node, because there is no case that multiple SAs are triggered simultaneously for the proposed modulation strategy. Assume the human locates at the angular bisector line of the area which is consist of multiple SAs, the method of human position localization and error analysis are same with that mentioned above.

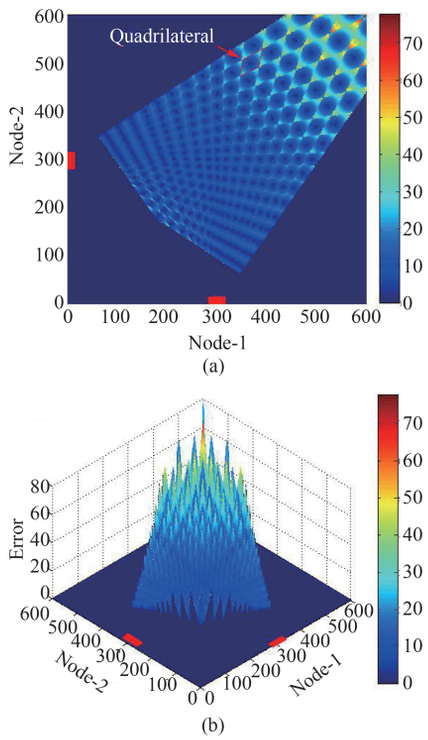

Fig. 5 The error analysis of the two nodes human localization equipment (a) Plane diagram of error analysis, (b) 3D diagram of error analysis.
图5 两节点人体定位装置的误差分析 (a) 误差分析结果平面图,(b) 误差分析结果三维图。

3 Experiment and discussion

In order to verify the proposed FOVs modulation strategy and the node, the human position localization experiments have been done. According to the setup which is shown in Fig. 4, we set two nodes in a 600 cm×600 cm square area, and the coordinates of node-1 and node-2 are (300, 0) and (0, 300) respectively. Before the experiments, the directions of two nodes should be calibrated to make the symmetry axes of detection areas of two nodes are perpendicular. And they are also perpendicular to the sidelines of the square area. The target human walks along the predefined route on the ground, stop in eight setting positions and do some minor movement. The speed is about 1 m/s. Record the output signals of the PIRs and then determine their states. The states determined processes can be seen in Fig. 6.

The original signal of a PIR is shown in Fig. 6(a). The signal is denoised by using the wavelet soft threshold noise reduction method. The denoised signal is shown in Fig. 6(b). The absolute value of the denoised signal is calculated, as shown in Fig. 6(c). But this process can introduce some interference points into the signal. The interference points are emphatic marked by red boxes, as shown in Fig. 6(c). In order to reduce the impact of the interference points, the signal should be smoothed, as shown in Fig. 6(d). Set a threshold (15% of the maximum of signal). If the amplitude of the signal is larger than the threshold, set the amplitude to '1', else to

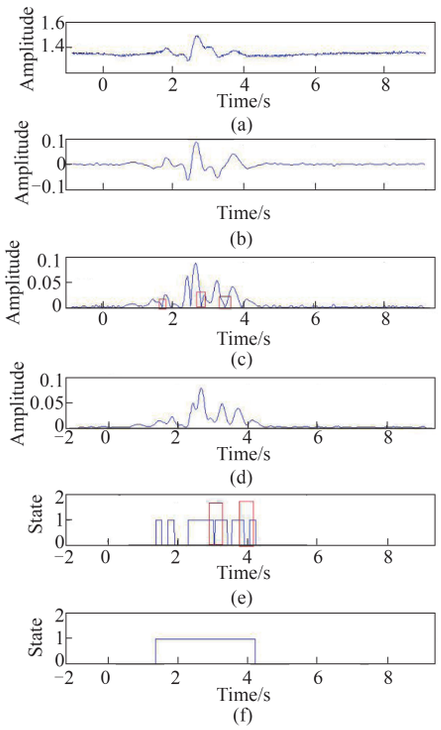

Fig. 6　The PIR states determined processes (a) the original signal, (b) denoise the signal by using wavelet soft threshold noise reduction method, (c) calculate the absolute values of the signal, (d) smoothing the signal, (e) set a threshold. If the amplitude of the signal larger than the threshold, set the amplitude to '1', else to '0', (f) further optimize the signal to determine the state of the PIR.

图6　热释电红外探测器状态确定过程 (a) 初始信号,(b)使用小波软阈值消噪法对信号降噪,(c)计算信号的绝对值,(d)平滑信号,(e) 设置阈值,如果信号的幅度大于阈值,则将信号的幅度置1,否则置0,(f) 进一步优化信号以确定热释电红外探测器的状态。

'0', as shown in Fig. 6(e). Some parts of state signal are misjudged due to the small absolute value, and they are marked by the red boxes, as shown in Fig. 6(e). Further optimize the signal to determine the final state of the PIR, as shown in Fig. 6(f). After the states of all PIRs are determined, the 'triggered' SAs can be determined. The recorded 'triggered' SAs of two nodes in experiments are shown in Table 4.

It can be seen from the Table 4, multiple SAs are take turn to be 'triggered' when the human stands at the setting positions and does some minor motions. The 'triggered' SAs of two nodes are listed in 2th and 3th columns of Table 4. According to the 'triggered' SAs of the node-1 and node-2, the θ_{1l} and θ_{2l} can be calculated by Eq. 4 or Eq. 5. The slopes k_{1l}, k_{2l} and two straight line expressions can be determined by Eq. 6 and Eq. 8 respectively. The estimation human position is the intersection of these two straight lines. The coordinates of eight setting positions and corresponding estimated positions are listed in 4th and 5th columns of Table 4. The errors are calculated and listed in 7th column of Table 4. It can be seen from the 7th column of Table 4, the minimum and maximum errors are about 4.42 cm and 16.91 cm respectively. The average error is about 9.34 cm. The minimum error 4.42 cm is smaller than 9cm and 32 cm which are reported in Ref. 15 and 13 respectively. The maximum error is similar to the maximum error which is reported in Ref. 15. The smaller minimum error may be due to the higher angle resolution. The node used in experiment can be seen in Fig. 7(a), the height of the node is 130 cm. Connect all the estimated points to form the estimation route. The estimated route and predefined route can be seen in Fig. 7(b). The predefined route and estimated route are represented by the red curve and blue curve respectively. It can be seen from the Fig. 7(b) that the estimated route is close to the predefined route.

Table 4　The result of the experiment
表4　实验结果

No.	Node-1	Node-2	Real /cm	Estimation/cm	Error/cm
r_1	S_{12}~S_{11}	S_6~S_8	(250,270)	(254.6,266.6)	8.09
r_2	S_{10}~S_9	S_8~S_9	(290,290)	(293.2,293.2)	4.47
r_3	S_8~S_7	S_9~S_{10}	(325,310)	(329.0,308.1)	4.42
r_4	S_7~S_6	S_{10}~S_{11}	(365,335)	(355.5,334.0)	9.57
r_5	S_6~S_5	S_{11}~S_{12}	(400,370)	(392.0,364.9)	9.44
r_6	S_5~S_4	S_{12}~S_{13}	(425,400)	(432.5,407.8)	10.86
r_7	S_5~S_4	S_{13}~S_{14}	(450,435)	(444.4,444.4)	10.94
r_8	S_4	S_{14}~S_{15}	(470,480)	(479.7,493.8)	16.91

In practice, some factors can affect the accuracy of human localization by using PIRs. For example, the other heating sources in FOV, human body temperature and

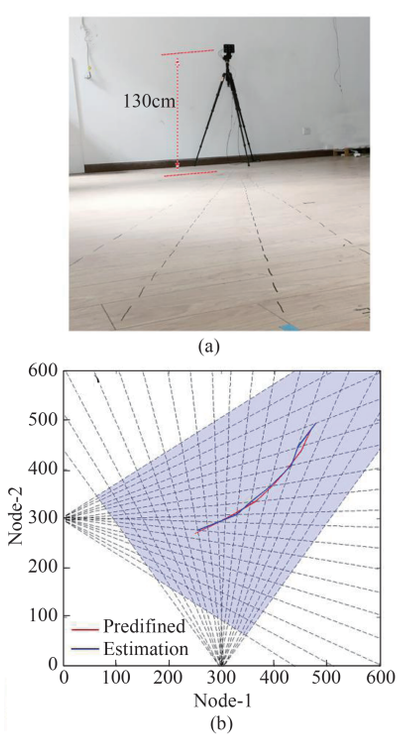

Fig. 7　The pyroelectric infrared human localization node and the experiment result (a) the pyroelectric infrared human localization node, (b) the predefined route and estimated route.

图7　热释电红外人体定位节点及实验结果 (a) 热释电红外人体定位节点, (b)预设路径及估计路径

so on. The dynamic infrared source, such as the moving animal, the air conditioner at working, head shaking heating system and the flying curtains, can affect the localization. Commonly, the pyroelectric signals caused by above heaters are different with that of human. The interference signals can be filtered by suitable filter. And the pattern recognition algorithms can be used to recognize whether the heater is human or not [16-17]. The temperature of body can also affect the detection of the PIR. The human body temperature is generally maintained at about 36°C. But it may change drastically after the human stay in cold or hot condition for a long time. Owing to the weaker pyroelectric signal, low body temperature may lead to incorrect localization. The high human body temperature doesn't affect the localization. And the problems caused by the body temperature may go away quickly once the body returns to a normal temperature[18]. Furthermore, the proposed method only can localize one human at one time. We are researching more advanced algorithms to enable the localization system to support multi-objective localization simultaneously.

4 Conclusion

In this paper, a field of views of pyroelectric infrared sensors modulation strategy is proposed. For the strategy, the angle resolution is related to the angle of FOV of localization system and the number of the PIRs. The proposed FOVs modulation strategy can improve the angle resolution without reduction of the detection distance of PIR. The theoretical localization error also be analyzed by using the least square estimation. The errors result from the hypothesis that the human is located at the angular bisector of the 'triggered' SA. In order to verify the proposed strategy. The human localization node which include nine PIRs is fabricated. The degrees of each SA, the FOV of each PIR and the detection area of the node are 4°, 36° and 68° respectively. The maximum theoretical error of the two nodes localization equipment in 600 cm×600 cm square area is about 70 cm. According to the state sequences of PIRs of the nodes, the target human position can be estimated. We set two nodes in a 600 cm×600 cm square area, and do the localization experiments. Eight positions are estimated. The minimum and maximum errors are about 4.42 cm and 16.91 cm respectively. The estimation route is close to the predefined route. The detection distance of the node is about 7 m. The experiment result indicates that the proposed FOVs modulation strategy is valid.

Acknowledge

This work supported by the National Key R&D plan (2016YFB0401500), R&D plan of Jiangsu science and technology department (BE2016173) and program B for outstanding PhD candidate of Nanjing University.

References

[1] Chodon P, Adhikari D M, Nepal G C, *et al*. Passive infrared (PIR) sensor based security system [J]. *International Journal of Electrical, Electronics & Computer System*, 2013, **14**(2): 1-5.
[2] Feng G D, Guo X M, Wang G L, Infrared motion sensing system for human-following robots [J]. *Sensors and Actuators A: Physical*, 2012, **186**: 1-7.
[3] Chowdhury M, Gao J B, Islam R. Robust human detection and localization in security applications [J]. *Concurrency and Computation-Practice & Experience*, 2017, **29**: e3977.
[4] Kakumanu P, Makrogiannis S, Bourbakis N. A survey of skin-color modeling and detection methods [J]. *Pattern Recognition*, 2007, **40**(3): 1106-1122.
[5] Meijer G C M, Vandrecht J, Dejong P C, *et al*. New concepts for smart signal processors and their application to PSD displacement transducers [J]. *Sensors and Actuators A: Physical*, 1992, **35**(1): 23-30.
[6] Tapia E M, Intille S S, Larson K. Activity recognition in the home using simple and ubiquitous sensors [C]//2nd International Conference on Pervasive Computing, 2004, **3001**: 158-175.
[7] Wilson D H, Atkeson C. Simultaneous tracking and activity recognition (STAR) using many anonymous, binary sensor [C]//Pervasive Computing, Proceedings, 2005, **3468**: 62-79.
[8] Chen L, Hoey J, Nugent C D, *et al*. Sensor-based activity recognition [J]. *IEEE Transactions on Systems Man and Cybernetics Part C-Applications and Reviews*, 2012, **42**(6): 790-808.
[9] Sun X Y, Luo W B, Meng J, *et al*. Monolithic pyroelectric infrared detectors using SiO2 aerogel thin films [J]. *Sensors and Actuators A: Physical*, 2015, **228**: 69-74.
[10] Wu Q Q, Wang Y Q, Ren S P. Low cost and anti-noise infrared device based on saw-tooth thermal isolation structure [J]. *Sensors and Actuators A: Physical*, 2017, **266**: 178-184.
[11] Luo W B, Wu Q Q, Wu C G, *et al*. Pb(ZrTi)0.98Mn0.02O3 weight ratio effects on the properties of Pb(ZrTi)0.98Mn0.02O3/P(VDF-TrFE) compostie film and infrared detectors [J]. *Journal of Materials Science: Materials in Electronics*, 2017, **28**(4): 3474-3480.
[12] Zhou W C, Li F M, Li D, *et al*. A human body positioning system with pyroelectric infrared sensor [J]. *International Journal of Sensor Networks*, 2016, **21**(2): 108-115.
[13] Jiang L, Zhang T, He F, et al, Preprocessing design in pyroelectric infrared sensor-based human-tracking system: on sensor selection and calibration [J]. *IEEE Transactions on Systems Man Cybernetics-Systems*, 2017, **47**(2): 263-275.
[14] Shankar M, Burchett J B, Hao Q, *et al*. Human-tracking systems using pyroelectric infrared detectors [J]. *Optical Engineering*, 2006, **45**(10): 106401.
[15] Feng G D, Guo X M, Wang G L. Infrared motion sensing system for human-following robots [J]. *Sensors and Actuators A: Physical*, 2012, **185**: 11-7.
[16] Gong W G, Wen K, He L F, *et al*. Human and Nonhuman Recognition Using Pyroelectric Infrared Detector [J]. *International Journal of Thermophysics*, 2012, **33**(10-11): 2237-2241.
[17] Zhao J D, Gong W G, Tang Y Z, *et al*. EMD-based symbolic dynamic analysis for the recognition of human and nonhuman pyroelectric infrared signals [J]. *Sensors*, **16**(1): 126.
[18] Gong J, Zhang Y, Zhou X. Pyro: Thumb-tip gesture recognition using pyroelectric infrared sensing [C]// UIST'17: Proceedings of The 30th Annual ACM Symposium On User Interface Software And Technology, 2017, 553-563.